Journal of Histochemistry & Cytochemistry 60(2) 97–109

DOI: 10.1369/0022155411433066
http://jhc.sagepub.com
SAGE

Three-Dimensional Microstructural Changes in Murine Abdominal Aortic Aneurysms Quantified Using Immunofluorescent Array Tomography

Sanaz Saatchi, Junya Azuma, Nishey Wanchoo, Stephen J Smith, Paul G. Yock, Charles A. Taylor, and Philip S. Tsao

Departments of Bioengineering (SS,PGY,CAT), Medicine (JA,PST), Mechanical Engineering (NW), and Molecular and Cellular Physiology (SJS), Stanford University, Stanford, California

Summary

This study investigated the spatial and temporal remodeling of blood vessel wall microarchitecture and cellular morphology during abdominal aortic aneurysm (AAA) development using immunofluorescent array tomography (IAT), a high-resolution three-dimensional (3D) microscopy technology, in the murine model. Infrarenal aortas of C57BL6 mice (N=20) were evaluated at 0, 7, and 28 days after elastase or heat-inactivated elastase perfusion. Custom algorithms quantified volume fractions (VF) of elastin, smooth muscle cell (SMC) actin, and adventitial collagen type I, as well as elastin thickness, elastin fragmentation, non-adventitial wall thickness, and nuclei amount. The 3D renderings depicted elastin and collagen type I degradation and SMC morphological changes. Elastin VF decreased 37.5% (p<0.01), thickness decreased 48.9%, and fragmentation increased 449.7% (p<0.001) over 28 days. SMC actin VF decreased 78.3% (p<0.001) from days 0 to 7 and increased 139.7% (p<0.05) from days 7 to 28. Non-adventitial wall thickness increased 61.1%, medial nuclei amount increased 159.1% (p<0.01), and adventitial collagen type I VF decreased 64.1% (p<0.001) over 28 days. IAT and custom image analysis algorithms have enabled robust quantification of vessel wall content, microstructure, and organization to help elucidate the dynamics of vascular remodeling during AAA development. (J Histochem Cytochem 60:97–109, 2012)

Keywords

immunofluorescence microscopy, three-dimensional microstructure, abdominal aortic aneurysm, elastin, smooth muscle cells, collagen, elastase, infrarenal aorta, quantitative image analysis

Abdominal aortic aneurysms (AAAs) are a prevalent and life-threatening degenerative disease in which there is a pathological dilation and possible rupture of the blood vessel. In the United States, AAAs occur in 4% to 9% of the population older than age 60 and are the cause of approximately 9000 deaths per year (Fleming et al. 2005; Humphrey and Taylor 2008). There are currently no specific therapies known to prevent the natural development of small asymptomatic AAAs (Thompson et al. 2006). For this reason, a better understanding of the pathological mechanisms that lead to aneurysm formation is needed to help guide therapeutic development.

The microstructural organization of a healthy elastic arterial wall consists of repeated medial lamellar units, comprised of elastin sheets interspersed with smooth muscle cells (SMCs) surrounded by collagen and other extracellular matrix (ECM) components (Clark and Glagov 1985; Dingemans et al. 2000;

Received for publication June 1, 2011; accepted November 11, 2011.

Corresponding Author:
Sanaz Saatchi, Department of Bioengineering, Stanford University, 318 Campus Drive, Room E350, Stanford, CA 94305.
E-mail: sanazsaatchi@gmail.com

O'Connell et al. 2008). However, during aneurysm development, this structural organization and integrity of the vessel wall is lost. Chronic inflammation, increased production of matrix-degrading proteinases, ECM destruction, and SMC depletion are integral to the disease process (Jacob et al. 2001; Thompson et al. 2006). Because SMCs are capable of directing the synthesis and repair of ECM components, depletion of these cells contributes significantly to the structural and functional deterioration of an aneurysmal aorta (Lopez-Candales et al. 1997; Thompson et al. 1997). Much remains to be elucidated about the spatial and temporal disorganization and depletion of elastin, SMCs, and collagen in the aortic wall during AAA progression.

Numerous animal models that mimic various components of the human disease process have been developed to gain a better understanding of the mechanisms underlying AAA development and progression. However, certain limitations do exist with previous studies. Many studies do not provide insight into the kinetics of the disease process because either a single time point or a relatively short time course is often evaluated. In addition, the imaging and microscopy tools frequently used, including immunofluorescence microscopy, confocal microscopy, electron microscopy, histology, and immunohistochemistry (IHC), provide only qualitative depictions of the disease process or basic subjective quantification. Additional weaknesses associated with these traditional microscopy technologies include limitations in resolution, quantitative analysis compatibility, and multiplexing capabilities. With these techniques, it is either difficult or impossible to gather high-resolution three-dimensional (3D) volumetric information. Three-dimensional volumetric information has the potential to provide great insight into the structure and organization of the tissue microarchitecture and cellular content, which may help elucidate the disease mechanism.

The purpose of this study is to apply a novel high-resolution 3D microscopy technology, called immunofluorescent array tomography (IAT), to study 3D microstructural changes in the murine elastase-perfusion aneurysm model (Anidjar et al. 1990; Micheva and Smith 2007). With IAT, arrays of ultrathin serial sections are generated that undergo numerous cycles of antibody staining and imaging to identify multiple targets of interest in a single sample using immunofluorescence microscopy. IAT is superior to existing imaging techniques in terms of spatial resolution, quantitative analysis compatibility, specificity, and multiplexing capabilities (Micheva and Smith 2007; Saatchi et al. 2011). Furthermore, 3D visualization of tissue and cellular ultrastructure using IAT will provide a unique perspective on aneurysm development for the first time. In our studies, we qualitatively and quantitatively describe both the spatial and temporal changes in the microarchitecture and cellular morphology of the murine blood vessel wall during AAA development.

Materials and Methods

Animal Studies

All animal experiments were approved by the Administrative Panel on Laboratory Animal Care at Stanford University. Eight- to 10-week-old C57BL6 mice were used for all studies with N=20 (n=4 per group).

Aneurysm Model: Elastase-Perfusion

Methods used for the elastase-perfusion procedure have been previously described (Azuma et al. 2009). Briefly, mice were anesthetized using 2.5% isoflurane, and a midline abdominal incision was made to expose the abdominal aorta extending from the left renal vein to the trifurcation. Aortic branches were ligated, and additional temporary ligatures were placed at the proximal aortic region (distal to the renal arteries) and at the distal aortic region (proximal to the trifurcation). After an aortotomy was performed in the distal aortic region, 1.5 U/ml of type I porcine pancreatic elastase in saline (specific activity 5 U/mg protein; E1250; Sigma Chemical Co., St. Louis, MO) was perfused into the aorta at 100 mm Hg for 5 min. The sham-operated control groups underwent the same procedure with an infusion of heat-inactivated elastase, in which the elastase was inactivated by 80C heat treatment for 30 min. The aortotomy was repaired, the temporary ligatures at the proximal and distal aortic regions were removed, and the wound was closed. Video microscopy was used to obtain digital images of the infrarenal aorta before and after elastase-perfusion, which were used to measure the external aortic diameter. At day 28, all elastase-treated mice developed infrarenal AAAs, defined as at least a 100% increase in aortic diameter from pre-elastase perfusion to time of sacrifice (Pyo et al. 2000; Sinha et al. 2006).

Sample Harvesting

Mice were euthanized by exsanguination under 2.5% isoflurane at the designated time points of day 0, as well as 7 and 28 days after infusion of elastase or heat-inactivated elastase. A midline abdominal incision was made to expose the abdominal aorta. A solution consisting of 0.15 ml xylocaine (2%), NaCl (0.9%), and heparin (100 U/ml) was injected into the left ventricle to prevent vasospasm and blood clotting (Davies and Gordon 2005). Saline was injected into the left ventricle at 100 mm Hg. Temporary ligatures were placed at the proximal and distal aortic regions. An aortotomy was performed in the infrarenal aorta, and 4% paraformaldehyde (16% Paraformaldehyde, EM Grade; Electron Microscopy Sciences, Hatfield, PA) in 0.01 M phosphate-buffered saline (PBS) was perfused into

the aorta at 100 mm Hg through a perfusion catheter. The perfusion catheter and temporary ligatures were removed. A suture was placed on the left renal artery for orientation purposes. Video microscopy was used to obtain digital images of the infrarenal aorta both before and after pressure-perfusion fixation with 4% paraformaldehyde. The aorta was harvested and fixed in 4% paraformaldehyde with 2.5% sucrose at 4C overnight. The anterior surface of the infrarenal aorta was marked with blue dye for orientation purposes. The sample was then cut at the point of maximum external diameter between the left renal artery and trifurcation. The control and heat-inactivated elastase sham-operated control samples were cut at an approximately similar location. The proximal portion of the sample was processed for IAT, whereas the distal portion was processed for histology and IHC. For IAT processing, the sample was dehydrated using a graded ethanol series, infiltrated in London Resin White resin (LR White resin, Medium Grade; SPI Supplies, West Chester, PA) for 3 to 4 hr at room temperature, and then embedded in fresh LR White resin for overnight polymerization at 51 to 53C (Micheva and Smith 2007). Standard processing methods were used for Elastic van Gieson (EVG) staining of elastin and immunohistochemical staining of smooth muscle cell actin (SMCA) and collagen type I in paraffin sections.

Array Generation

Serial sections were cut from the LR White resin block using an ultramicrotome (Leica EM UC6, Leica Microsystems, Wetzlar, Germany, and Jumbo Histo Diamond Knife, Diatome, Hatfield, PA) to generate arrays, or ribbons, comprised of individual ultrathin sections of 200 nm thickness (Micheva and Smith 2007). Ribbons were then transferred onto a coverslip.

Staining

A glycine pretreatment was followed by blocking solution for 30 min (Micheva and Smith 2007). Blocking solution consisted of 0.05% Tween (Tween 20; Acros Organics, Morris Plains, NJ) and 0.1% bovine serum albumin (BSA Fraction V; Fisher Scientific, Pittsburgh, PA) in Tris buffer. In the first staining cycle, actin alpha 2 smooth muscle primary antibody (host species: rabbit; isotype: IgG; manufacturer's concentration: 200 µg/ml; catalogue number: NB600-531; lot number: 100105; Novus Biologicals, Littleton, CO) at 20 µg/ml and collagen type I primary antibody (Col1A1 [D-13]; host species: goat; isotype: IgG; manufacturer's concentration: 200 µg/ml; catalogue number: SC-25974; lot number: F2609; Santa Cruz Biotechnology, Santa Cruz, CA) at 10 µg/ml in the described blocking solution were applied directly onto the ribbons, overnight at 4C (Saatchi et al. 2011). Ribbons were washed several times with PBS. The secondary antibodies, donkey anti-rabbit Alexa Fluor 488 (isotype: IgG; manufacturer's concentration: 2 mg/ml; catalogue number: A-21206; lot number: 556439; Invitrogen, Carlsbad, CA) and donkey anti-goat Alexa Fluor 647 (isotype: IgG; manufacturer's concentration: 2 mg/ml; catalogue number: A-21447; lot number: 552224; Invitrogen), were applied directly to the ribbons at 10 µg/ml in blocking solution for 30 min at room temperature (Saatchi et al. 2011). Ribbons were washed several times with PBS, then with distilled water. Finally, the coverslip, with attached ribbon, was mounted onto a slide using mounting medium with DAPI (SlowFade Gold Antifade Reagent with DAPI; Invitrogen Molecular Probes, Carlsbad, CA).

After completion of cycle 1 imaging, antibodies were eluted from the samples. Briefly, an elution solution, 0.1% sodium dodecyl sulfate (SDS) in 0.2 M NaOH, was applied directly to the ribbons for 15 min (Micheva and Smith 2007). The ribbons then underwent a second staining cycle. Again, ribbons were pretreated with glycine, followed by blocking solution for 30 min. Elastin primary antibody (host species: rabbit; isotype: IgG; manufacturer's concentration: 500 µg/ml; catalogue number: AB21610; lot number: 863096; Abcam, Cambridge, MA) at 10 µg/ml in blocking solution was applied overnight at 4C. Donkey anti-rabbit Alexa Fluor 488 secondary antibody was again applied at 10 µg/ml dilution in blocking solution for 30 min at room temperature. Finally, ribbons were mounted onto slides using mounting medium with DAPI.

In addition, standard methods were used for EVG staining of elastin and immunohistochemical staining of SMCA and collagen type I. Primary antibodies used for IAT were also used for IHC at the following concentrations: actin alpha 2 smooth muscle primary antibody at 1 µg/ml and collagen type I primary antibody at 5 µg/ml.

Microscopy and Automated Image Acquisition

Images were acquired using a Zeiss fluorescence microscope (Axio Imager.Z1 Upright Fluorescence Microscope, Plan—Apochromat 10×/0.45 NA DIC II objective, Plan—Apochromat 63×/1.4NA DIC II oil objective, AxioCam HRm CCD 1.0× camera, and AxioVision 4.7 software; Zeiss, Jena, Germany) with a motorized stage for automated image acquisition. Representative areas of both the anterior and posterior vessel wall regions were selected for 63× imaging. Each imaging cycle produced a series of individual two-dimensional (2D) images, with each image corresponding to a single section within the array of serial sections. Pixel dimension in each 63× image was 100 nm, and the image size was 1360 pixels (x-axis), 1040 pixels (y-axis), and 2 pixels (z-axis),

corresponding to dimensions of 136 μm (x), 104 μm (y), and 0.2 μm (z) for each image slice. The number of image slices per sample ranged from 10 to 30 slices with an average of 23 slices per sample. Therefore, the average total volume size was 136 μm (x), 104 μm (y), and 4.6 μm (z).

Image Processing: Segmentation and Registration

ImageJ (National Institutes of Health, Bethesda, MD) was used for image segmentation by separating the colorimetric Red-Green-Blue (RGB) images into a series of gray-scale images, with a separate gray-scale image series corresponding to each individual tissue constituent. Following segmentation, all image series from the first imaging cycle were aligned (Micheva and Smith 2007; Saatchi et al. 2011). Subsequently, the image stack acquired during the second imaging cycle was registered to that from the first cycle, and then aligned, to create a composite image series with integrated information across all cycles (Micheva and Smith 2007; Saatchi et al. 2011).

Image Analysis

Three-dimensional qualitative renderings of the 63× image sets were created using AxioVision software (AxioVision 4.7; Zeiss) for both the anterior and posterior vessel wall regions. Custom algorithms using MATLAB (MATLAB R2007b; MathWorks, Natick, MA) were developed for quantitative analysis of microstructure and cellular morphology (Saatchi et al. 2011). Aligned segmented gray-scale image series were used for individual tissue constituent analysis, specifically elastin, SMCA, collagen type I, and nuclei. Objects, defined as a set of pixels that formed a connected group, were identified and two regions of interest (ROIs) were defined and applied across the series of images. The media ROI extended from the luminal edge of the innermost elastin layer to the adventitial edge of the external elastic lamina. The adventitia ROI outlined a small region of the adventitia adjacent to the media. Volume fractions of medial elastin and SMCA, as well as adventitial collagen type I, were measured (Saatchi et al. 2011).

The structure and organization of elastin were analyzed by quantifying the thickness of elastin, non-adventitial wall thickness, and elastin fragmentation. By evaluating changes in the binary pixel intensity profile across a set of five lines extending in the radial direction across the media, elastin thickness and non-adventitial wall thickness were measured (Saatchi et al. 2011). Finally, elastin fragmentation was also determined to quantitatively describe the structural organization of elastin. An elastin fragmentation index was defined as the ratio of the number of elastin objects to the area, or total pixel count, of elastin objects (Saatchi et al. 2011).

Finally, the number of nuclei within the media ROI was evaluated to investigate changes in cellular amount.

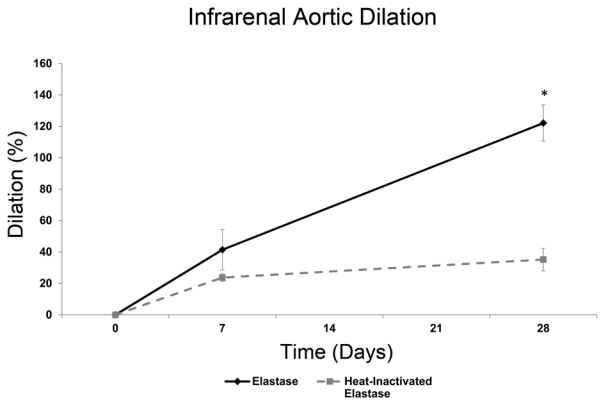

Figure 1. Aneurysmal aortic dilation. Infrarenal aortic external diameter was measured to calculate aortic dilation after elastase and heat-inactivated elastase treatment. At day 28, aortic dilation was significantly larger (*$p<0.01$) in the elastase-treated group than in the heat-inactivated elastase-treated group. The day 28 elastase group was considered aneurysmal due to an increase in aortic diameter greater than 100% from the pre-elastase treatment time point. Mean ± SEM, $N=20$, $n=4$ per group.

Statistical Analysis

All data are presented as mean ± standard error (SEM) with $N=20$ ($n=4$ per group; day 0, day 7 elastase, day 7 heat-inactivated elastase, day 28 elastase, day 28 heat-inactivated elastase). Student's *t*-test was performed to assess the statistical significance of differences measured across the anterior and posterior vessel wall regions, as well as across the elastase-treated and heat-inactivated elastase-treated groups. One-way analysis of variance (ANOVA) was performed using SAS (SAS Institute, Inc., Cary, NC) to determine the statistical significance of changes measured over time.

Results

Infrarenal Aortic Dilation

Aortic dilation was calculated using infrarenal aortic external diameter measurements (Fig. 1). As expected with the elastase-perfusion model, the infrarenal aortic diameter increased over time. The slight dilation observed in the heat-inactivated elastase-treated group at day 7 is likely a result of the mechanical damage imposed on the vessel wall by the pressurized infusion process. At both day 7 and day 28 ($p<0.01$), aortic dilation is larger in the elastase-treated

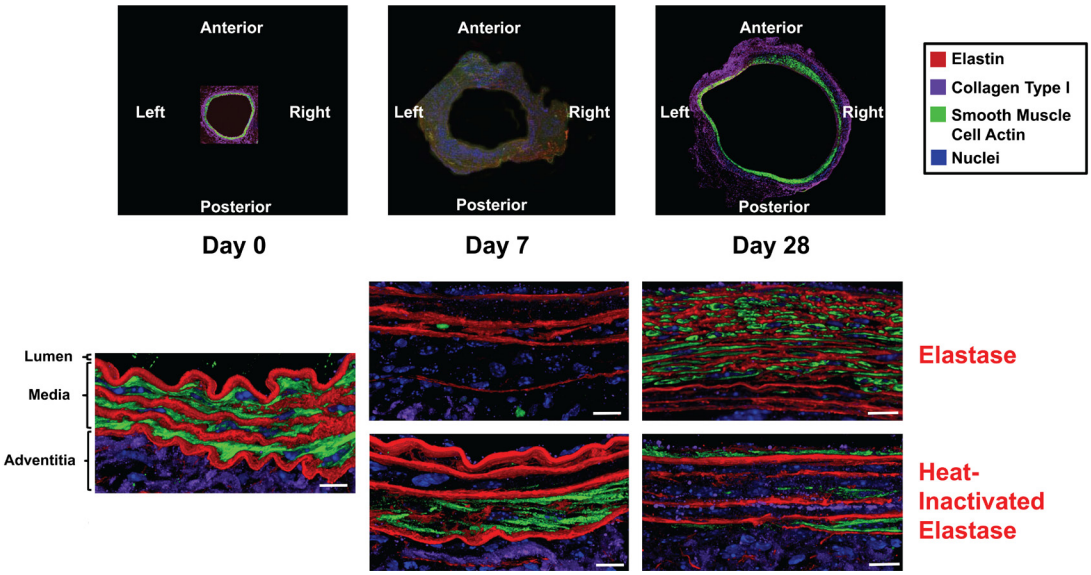

Figure 2. Microstructural and cellular changes during aneurysm development. Three-dimensional volume renderings (x-y cross-sectional view) produced by immunofluorescent array tomography (IAT) enabled temporal investigation into microstructural, organizational, and cellular remodeling during aneurysm development. In the elastase group, elastin degradation was described by the loss of elastin thickness, density, and organization, whereas elastin fragmentation and non-adventitial wall thickness increased over the 28-day time course. Dynamic changes in smooth muscle cells (SMCs) were observed with a dramatic loss of smooth muscle cell actin (SMCA) at day 7 and a return in suppressed amounts at day 28. Adventitial collagen type I degradation was also prevalent over the 28-day time course. In the heat-inactivated elastase group, minimal changes in elastin were observed as elastin lamellae thickness, density, and organization remained relatively constant across time. Similar trends as those seen in the elastase group, specifically related to the decrease and return of SMCA and loss of adventitial collagen type I, were observed in the heat-inactivated elastase group. Top panel: 10× magnification; bottom panels: 63× magnification. Scale bar represents 10 μm, three-dimensional renderings with average total volume size of 136 μm (x), 104 μm (y), and 4.6 μm (z).

group than in the heat-inactivated elastase-treated group. The day 28 elastase group is considered aneurysmal, as defined by dilation greater than 100% from pre-elastase treatment (Fig. 1) (Pyo et al. 2000; Sinha et al. 2006).

Qualitative Image Analysis

IAT. Temporal and spatial (data not shown) changes in microstructure and cellular morphology that occurred during AAA development were detailed with 3D renderings produced by IAT (Fig. 2). At day 0, the media possessed a well-organized structure. The elastin lamellae were thick, dense, unfragmented, and uniformly spaced. SMCs were elongated in morphology and uniformly oriented, and they possessed an abundant amount of SMCA with a diffuse configuration. In addition, there was an abundant amount of collagen type I found predominantly in the adventitia.

In the day 7 elastase group, elastin lamellae were less organized, heterogeneously spaced, and less dense than day 0. There was a dramatic change in SMCs with the substantial loss of SMCA. In addition, adventitial collagen type I content also decreased. In the day 7 heat-inactivated elastase group, elastin lamellae were similar to day 0 in terms of organization, spacing, and density. Similar to the day 7 elastase group, SMCA and adventitial collagen type I decreased relative to day 0.

In the day 28 elastase group, the organized medial structure seen at day 0 was absent. Elastin layers were much thinner, heterogeneously spaced, less dense, more fragmented, and disorganized relative to both day 0 and day 7. Although the majority of elastin possessed a thin, fragmented, and compressed appearance, there did appear to be minimal amounts of intact elastin in the outer medial region. Furthermore, the overall vessel wall thickness increased likely as a result of neointima formation. Another dramatic change was the increase in SMCA content relative to day 7. Although SMCA reappeared at day 28, it returned in diminished amounts and altered morphology relative to day 0. In contrast to day 0, SMCA at day 28 possessed a discrete, specific, and localized configuration. Overall, the SMCs possessed non-uniform orientation and morphology. Finally, adventitial collagen type I content remained reduced relative

to day 0. By contrast, in the day 28 heat-inactivated elastase group, the media retained the organized structure seen at day 0. Elastin lamellae thickness, spacing, density, and organization were similar to both day 0 and day 7 heat-inactivated elastase groups. Unlike the day 28 elastase group, elastin was not fragmented and disorganized. In addition, the reappearance of SMCA was also apparent in this group, albeit to a lesser degree. From the IAT volumetric renderings, adventitial collagen type I content in the day 28 heat-inactivated elastase group remained suppressed relative to day 0.

Histology and IHC. Histological and immunohistochemical characterization of elastin, SMCA, and adventitial collagen type I validated IAT qualitative image analysis findings (Fig. 3A–C). As seen with IAT, EVG results depict, with less detail, the overall decrease in elastin thickness and organization and the increase in non-adventitial wall thickness that occurred during aneurysm development in the elastase group (Fig. 3A). Again, temporal changes in elastin thickness and organization in the heat-inactivated elastase group were minimal relative to those in the elastase group.

The dynamic changes in SMCA content were also confirmed by IHC (Fig. 3B). Although IHC did not provide enough resolution to detect changes in SMC orientation and morphology, it was apparent that SMCA content decreased from day 0 to day 7 and subsequently increased from day 7 to day 28 in both the elastase and heat-inactivated elastase groups.

Finally, collagen type I was also characterized by IHC (Fig. 3C). In both the elastase and heat-inactivated elastase groups, adventitial collagen type I content at days 7 and 28 was reduced relative to day 0.

Quantitative Image Analysis

Global Analysis: Volume Fractions of Elastin, SMCA, and Collagen Type I. Using IAT and custom image analysis algorithms, volume fractions of elastin, SMCA, and adventitial collagen type I were quantified, both spatially (data not shown) and temporally, to better understand the aneurysmal degeneration process (Fig. 4). At each time point, elastin, SMCA, and adventitial collagen type I volume fraction values were not significantly different ($p>0.05$) across the anterior and posterior vessel wall regions in each group (day 0, day 7 elastase, day 7 heat-inactivated elastase, day 28 elastase, day 28 heat-inactivated elastase; $n=4$ per group). Therefore, the anterior and posterior volume fraction values were combined to assess temporal differences across the elastase and heat-inactivated elastase groups.

Elastin volume fraction decreased over time, with the largest decrease occurring from day 0 to day 7 in both groups (Fig. 4A). Elastin volume fraction decreased 33.9% ($p<0.01$) and 7.4% in the elastase and heat-inactivated elastase groups, respectively, from day 0 to day 7, followed by a 5.4% and 2.7% decrease in the elastase and heat-inactivated elastase groups, respectively, from day 7 to day 28. In the elastase group only, elastin volume fraction remained significantly suppressed at day 28 ($p<0.01$) relative to day 0. Differences in elastin volume fraction values across the elastase and the heat-inactivated elastase groups were significant at both day 7 ($p<0.05$) and day 28 ($p<0.05$).

The dynamic changes in SMCA volume fraction (Fig. 4B) were quantified as a 78.3% and 73.6% decrease in the elastase and heat-inactivated elastase groups, respectively, from day 0 to day 7, followed by a 139.7% and 29.6% increase in the elastase and heat-inactivated elastase groups, respectively, from day 7 to day 28. The rate of SMCA volume fraction increase from day 7 to day 28 was higher in the elastase than in the heat-inactivated elastase group. A significant difference in each pairwise comparison was observed in the elastase group only ($p<0.001$, days 0–7; $p<0.001$, days 0–28; $p<0.05$, days 7–28). In the heat-inactivated elastase group, SMCA volume fractions at days 7 ($p<0.001$) and 28 ($p<0.001$) were significantly different from those at day 0 only.

Adventitial collagen type I volume fraction (Fig. 4C) decreased 70.8% ($p<0.001$) and 68.1% ($p<0.001$) in the elastase and heat-inactivated elastase groups, respectively, from day 0 to day 7, followed by a 23.1% and 63.3% increase in the elastase and heat-inactivated elastase groups, respectively, from day 7 to day 28. Despite this recovery in collagen type I, volume fraction levels remained significantly suppressed in both the elastase ($p<0.001$) and heat-inactivated elastase ($p<0.01$) groups at day 28 relative to day 0.

Structural Analysis: Elastin Thickness and Non-Adventitial Wall Thickness

Elastin Thickness. As previously described, the media ROI used to measure structural metrics, such as elastin and non-adventitial wall thickness, extended from the luminal edge of the innermost elastin layer to the adventitial edge of the external elastic lamina. In the elastase group, elastin thickness (Fig. 5A) decreased across all time points. The largest decrease in elastin thickness in the heat-inactivated elastase group occurred from day 0 to day 7 with an 8.5% decrease. The rate of elastin thickness decrease across all time points was higher in the elastase than in the heat-inactivated elastase group.

Non-Adventitial Wall Thickness. The largest increase in non-adventitial wall thickness occurred from day 7 to day 28 in both the elastase and heat-inactivated elastase groups

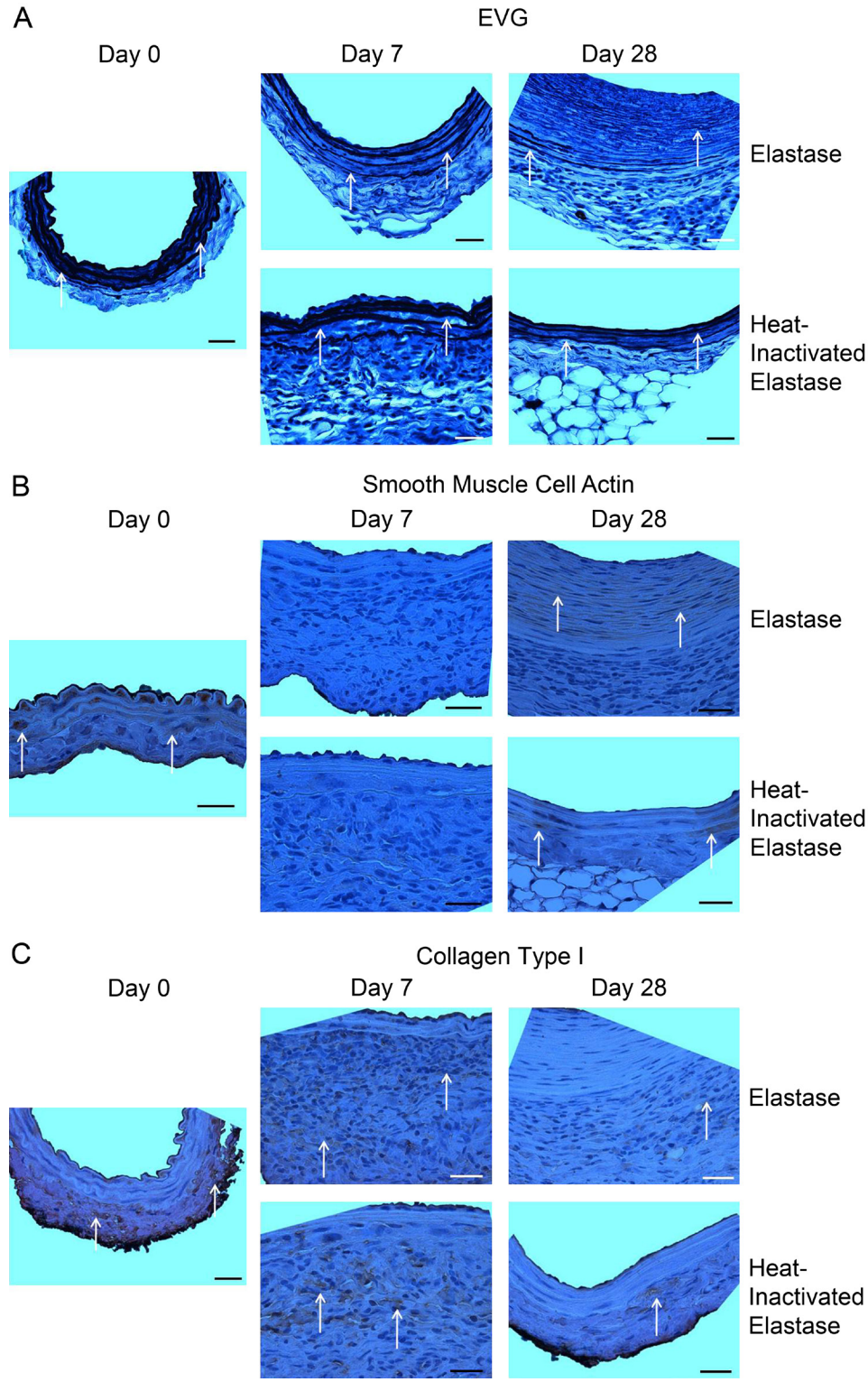

Figure 3. Histology and immunohistochemistry. Histological and immunohistochemical characterization of elastin (A), smooth muscle cell actin (SMCA) (B), and adventitial collagen type I (C) validated immunofluorescent array tomography (IAT) findings. (A) Elastic van Gieson (EVG) results depict the loss of elastin thickness and organization and the increase in non-adventitial wall thickness that occurred during aneurysm development in the elastase group. Elastin lamellae structure and organization in the heat-inactivated elastase group were relatively constant. Arrows highlight elastin stained by EVG. (B) SMCA content changed dynamically with a decrease from day 0 to day 7 and subsequent increase from day 7 to day 28 in both the elastase and heat-inactivated elastase groups. Arrows highlight regions with positive staining for SMCA. (C) In both the elastase and heat-inactivated elastase groups, adventitial collagen type I content at days 7 and 28 decreased relative to day 0. Arrows highlight areas with positive staining for collagen type I. Orientation of all images: lumen at top and adventitia at bottom of image. Images taken at 63× magnification with scale bar representing 25 μm.

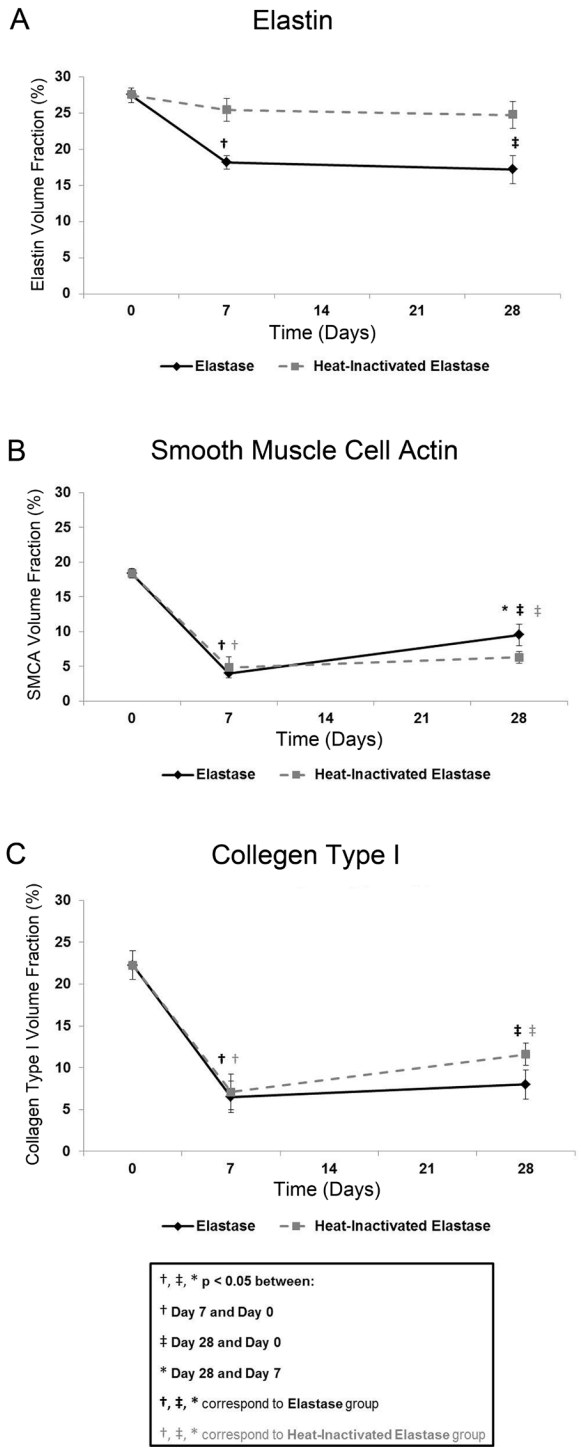

Figure 4. Global analysis: volume fractions of elastin, smooth muscle cell actin (SMCA), and collagen type I. (A) A significant decrease in elastin volume fraction at day 7 and day 28 relative to day 0 was observed in the elastase group only. (B) SMCA volume fraction decreased significantly from day 0 to day 7 and returned at day 28, although still significantly suppressed relative to day 0, in both groups. (C) The largest decrease in adventitial collagen type I volume fraction occurred from day 0 to day 7 and remained significantly suppressed at day 28, relative to day 0, in both groups. Mean ± SEM, N=20, n=4 per group.

(Fig. 5B). The rate of wall thickness increase from day 7 to day 28 was higher in the elastase than in the heat-inactivated elastase group.

Organizational Analysis: Elastin Fragmentation. Elastin fragmentation (Fig. 6) in the elastase group increased 86.4% from day 0 to day 7, followed by a 194.9% (p<0.01) increase from day 7 to day 28. The largest change in elastin fragmentation in the heat-inactivated elastase group also occurred from day 7 to day 28 with a 54.6% increase. In the elastase group only, elastin fragmentation at day 28 (p<0.001) was significantly higher than that at day 0. Differences in elastin fragmentation across the elastase and the heat-inactivated elastase groups were significant at both day 7 (p<0.001) and day 28 (p<0.05).

Cellular Analysis: Nuclei Amount. Nuclei amount, or the number of nuclei objects within the media ROI, increased over time in the elastase group (Fig. 7). Changes in nuclei amount were quantified as a 35.3% increase and 18.3% decrease in the elastase and heat-inactivated elastase groups, respectively, from day 0 to day 7, followed by a 91.5% (p<0.01) and 85.7% increase in the elastase and heat-inactivated elastase groups, respectively, from day 7 to day 28. The rate of increase in nuclei amount from day 7 to 28 was higher in the elastase than in the heat-inactivated elastase group. In the elastase group only, the number of nuclei at day 28 (p<0.01) was significantly higher than that at day 0. Because the nuclei were identified by DAPI staining, specific cell type was not verified with this metric. Therefore, the increase in nuclei amount within the media ROI may, in part, be due to an influx of various cell types for vessel wall repair.

Discussion

Although the elastase-perfusion AAA murine model, in addition to other aneurysm animal models, has been widely used to study aneurysm development, greater insight into the disease mechanism may be gained from investigations into the finer details of microstructural remodeling. Previous studies have provided limited information about the kinetics of the disease process because only a single time point was evaluated, a shorter time course was studied, or imaging tools with limited capabilities were used. Some limitations of commonly used imaging and microscopy tools include inferior resolution, depth-dependent resolution, subjective and categorical quantitative analysis, limited multiplexing capabilities, and 2D instead of 3D visualization capabilities. The strengths, advantages, and unique capabilities provided by IAT have been previously described (Micheva and Smith 2007; Saatchi et al. 2011). Briefly, IAT produces 3D colorimetric immunofluorescence microscopy images with improved lateral and axial resolution, specificity in staining, simple segmentation capabilities, amenability to quantification, and enhanced

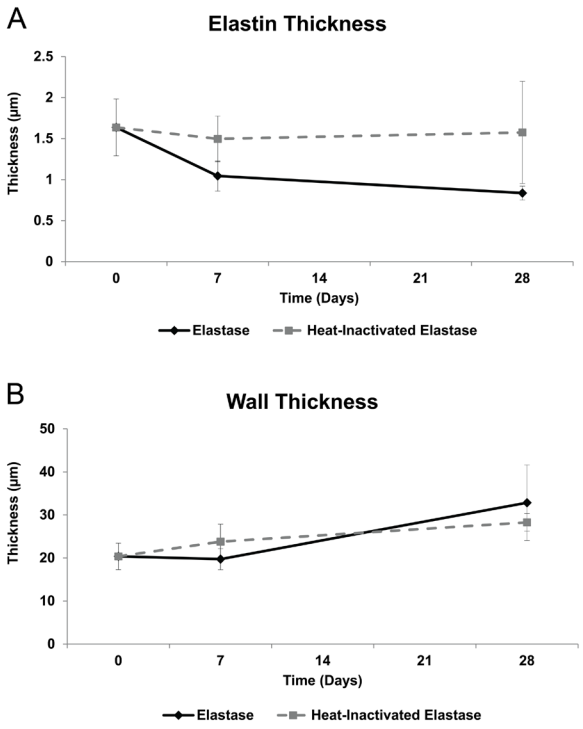

Figure 5. Structural analysis: elastin thickness and non-adventitial wall thickness. (A) Elastin thickness decreased across all time points in the elastase group. The overall decrease in elastin thickness from day 0 to day 28 was larger in the elastase group (48.9%) than in the heat-inactivated elastase group (3.8%). (B) Non-adventitial wall thickness increased over time, with the largest increase (66.4%) occurring from day 7 to day 28 in the elastase group. Mean ± SEM, *N*=20, *n*=4 per group.

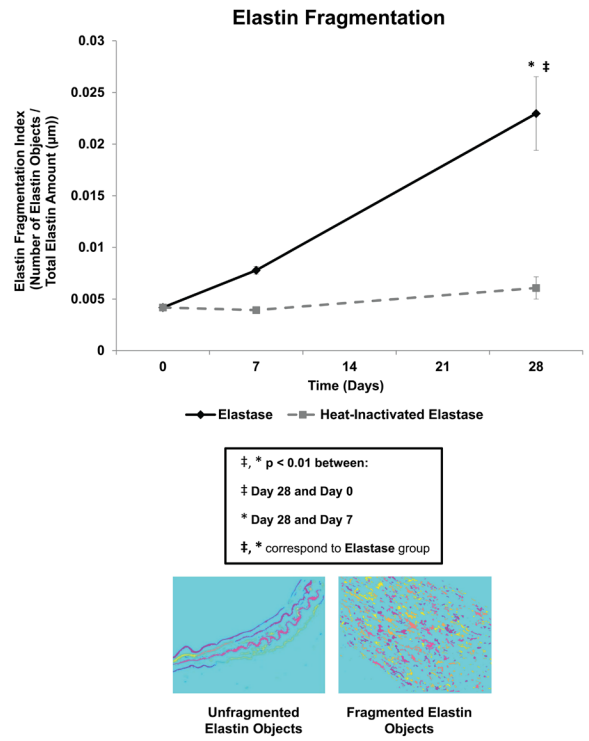

Figure 6. Organizational analysis: elastin fragmentation. In the elastase group only, elastin fragmentation increased significantly over time, with day 28 elastin fragmentation being significantly higher than both day 0 and day 7. Mean ± SEM, *N*=20, *n*=4 per group.

multiplexing capabilities. We have addressed many of the commonly encountered limitations associated with traditional microscopy tools by using IAT to produce 3D high-resolution qualitative and quantitative depictions of tissue microarchitecture and cellular morphology during aneurysm development. By evaluating multiple time points and various anatomical locations in the elastase-perfusion murine model, we explored the kinetics of the disease process and any potential heterogeneity in vessel wall deterioration. Because we did not find significant heterogeneity in regional vessel wall deterioration, the findings focused on temporal remodeling of the vessel wall constituents.

Elastin is a key tissue constituent that plays an integral role in maintaining the organization and structural integrity of the blood vessel wall. This study has described elastin remodeling, both qualitatively and quantitatively, during aneurysm development in the murine elastase-perfusion AAA model at a higher order of detail. Qualitatively, these studies have illustrated how elastin transitions from thick, dense, lamellae with an organized structure to thin, less dense, highly fragmented, and disorganized elastin within 28 days of elastase treatment. The superior resolution of IAT was capable of distinguishing individual, thin, segments of elastin at day 28, many of which may be newly formed elastin. In contrast, intact elastin in the outer region of the media may be residual portions of the original elastin layers. Furthermore, additional markers, such as a tropoelastin primary antibody, can also be incorporated into future studies to investigate the relative changes in tropoelastin synthesis across time. As an elastin precursor, tropoelastin measurements would describe the amount of substrate that possesses the potential to be cross-linked and assembled into elastin.

Previous studies primarily performed categorical and subjective quantitative analysis based on histological or immunohistochemical images with limited resolution (Dai et al. 2006). However, analysis using high-resolution IAT images enabled a more robust quantitative assessment of aneurysmal remodeling in terms of level of detail, minimized subjectivity, and detection capabilities. Quantitative assessment of elastin degradation focused not only on elastin amount but also on the structure and organization of elastin at various time points during aneurysm development. We have reported

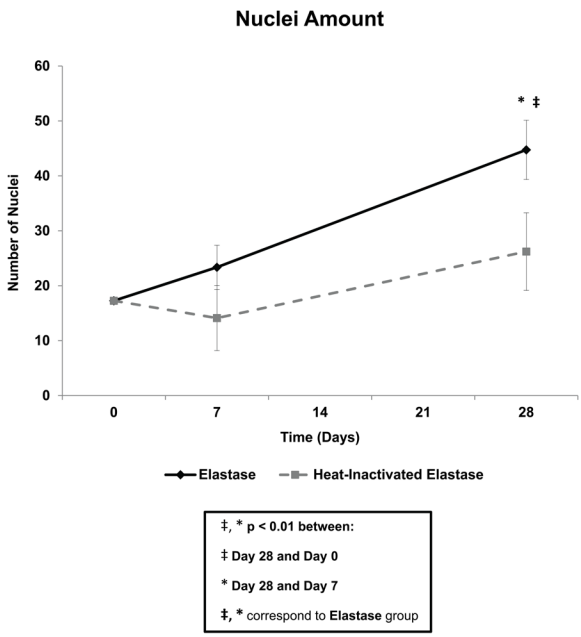

Figure 7. Cellular analysis: nuclei amount. The amount of nuclei increased across all time points in the elastase group. In the elastase group only, the number of nuclei at day 28 was significantly higher than that at day 0 and day 7. Mean ± SEM, N=20, n=4 per group.

an overall 37.5% loss in elastin volume fraction and 48.9% decrease in elastin thickness over the 28-day post-elastase treatment time course. In addition, the non-adventitial wall thickness increased 61.1% over 28 days, with the most dramatic change occurring from day 7 to day 28. Presumably, the abundant amount of neointima formation present at day 28 contributed to this increase in thickness. In addition to studying elastin content and structure, the organization of elastin was also investigated by quantifying elastin fragmentation for the first time. Elastin fragmentation increased 449.7% over the 28-day post-elastase time course, with the most dramatic increase occurring from day 7 to day 28. Fragmentation of elastin is an integral component of the aneurysmal disease process as it contributes to the loss of vessel wall structural integrity. The ability to now quantitatively characterize the kinetics of elastin degradation may help elucidate aneurysm pathology.

SMCs are of significant interest because they are involved in the synthesis of ECM molecules, as well as the expression of both proteinases and their inhibitors (Lopez-Candales et al. 1997). SMCA, a commonly used SMC lineage marker, was selected as the target of interest to enable the investigation of SMC content, morphology, and orientation during aneurysm development. Qualitatively, IAT illustrated cellular changes from an elongated morphology with abundant amounts of SMCA, to minimal amounts of SMCA at day 7, to a return of SMCA in a diminished amount and altered morphology 28 days after elastase treatment. These dynamic changes in SMCA amount may be related to variations in SMC functionality during the repair process.

IAT enabled quantification of the initial SMCA loss at day 7 as 78.3%, followed by an increase of 139.7% as SMCA returned 28 days after elastase treatment. Previous studies have found similar results when using the elastase-perfusion murine AAA model. Specifically, other studies have observed a similar dramatic loss of SMCA at day 7, as characterized by qPCR measurement of SMCA expression (Ailawadi et al. 2009). Furthermore, SMCA content in the heat-inactivated elastase group was also reduced at day 7 and day 28 relative to day 0. This SMCA loss in the heat-inactivated elastase group may be a result of the surgical procedure's mechanical impact on the vessel wall SMCs, as mechanical forces have previously been shown to stimulate SMC phenotype change (Owens et al. 2004; Rensen et al. 2007; Acampora et al. 2010).

Previous studies have suggested that SMCs undergo dynamic changes in phenotype during AAA development. These phenotypic changes correlate to adaptations in SMC functionality as the cells dedifferentiate from the contractile to the synthetic phenotype to proliferate and migrate to the injury site and synthesize ECM for vessel wall repair (Iwata and Sata 2008; Ailawadi et al. 2009). One hallmark of the transition from contractile to synthetic phenotype in SMCs is the loss of SMCA. Often, the loss of SMCA is coupled with other key characteristics, such as cell shape change, increased expression of matrix metalloproteinases 2 and 9, and increased expression of vimentin, to prove the transition in cell phenotype (Bunton et al. 2001; Ailawadi et al. 2009). Although additional IAT markers would be required to prove the SMC phenotypic change from contractile at day 0 to synthetic at day 7 to an altered contractile phenotype at day 28, the dynamic changes in SMCA content captured in this study support the theory of phenotypic change during aneurysm development. It should be noted that similar processes appear to occur in the heat-inactivated elastase group, albeit to a lesser degree. Thus, vascular SMC phenotypic switching alone may not be sufficient to elicit aneurysmal remodeling.

In addition to SMCA content, nuclei amount was also measured to further investigate the cellular response to aneurysm formation. The number of nuclei within the media increased 159.1% over the 28-day post-elastase time course. This overall increase in nuclei amount is indicative of enhanced cell content without discrimination of a specific cell type. Hence, the increased cell content may be due to both SMC proliferation and infiltration of various cell types, such as inflammatory cells, recruited for vessel wall repair.

Collagen type I is a major form of collagen found primarily in the vessel wall adventitia and provides tensile strength to the vessel. Because of the capabilities of IAT, collagen type I was able to be targeted specifically, in isolation of other collagen types. Qualitatively, IAT illustrated the loss in adventitial collagen type I over time. Overall, adventitial collagen type I decreased 64.1% over the 28-day post-elastase time course. It is important to note that this study focused on the remodeling of collagen type I, specifically, and concentrated on a subregion of the adventitia. The response of other types of collagen to AAA formation may differ from the results presented in this study.

In addition, it is interesting to note that the dynamic changes in adventitial collagen type I volume fraction are similar to those of SMCA volume fraction across the 28-day time course. The overall trends over time, as described by a decrease in volume fraction from day 0 to day 7 followed by a subsequent increase in volume fraction from day 7 to day 28, are similar across both metrics in both the elastase and heat-inactivated elastase groups. These results may indicate the presence of either a unidirectional or a bidirectional relationship between SMC phenotype and ECM composition and organization. SMC phenotypic changes may influence the degradation and synthesis of collagen type I, which are likely controlled, in part, by SMC expression of proteinases and their inhibitors, whereas collagen type I composition and organization have also been shown to influence SMC phenotype and SMC response to mechanical stimuli (Rensen et al. 2007).

Furthermore, previous findings regarding collagen type I levels within AAAs have been inconsistent (Menashi et al. 1987; Rizzo et al. 1989; Cho et al. 2010). The present study supports recent findings by Cho et al. (2010) in which collagen type I levels were shown to decrease in the elastase-perfusion Sprague Dawley rat model by day 14. Results at 28 days were not reported as the study was concluded 14 days after elastase perfusion. The loss of collagen type I is a significant component of aneurysm pathogenesis and is thought to lead to eventual aneurysm rupture. Therefore, it is important to have an accurate understanding of collagen remodeling during aneurysm development.

Although the present study uses IAT to investigate the dynamic mechanism of AAA development and progression, certain limitations do exist. Because IAT is an ex vivo technique, the same animals cannot be evaluated across all time points. This limitation can be addressed by evaluating a larger sample size of animals per group. In addition, characterization of adventitial collagen type I may have been influenced by the dissection technique. This limitation was addressed by analyzing a small region of the adventitia adjacent to the media. Furthermore, the current image analysis methods analyzed all nuclei within the media, as opposed to isolating the nuclei of SMCs only. Other cell types may have been incorporated into nuclei quantifications. Differentiation of cell types can be explored by including markers of various cells into future studies. The incorporation of additional markers would require experimentation and optimization of staining conditions for each antibody added. Moreover, the power of this technique can be further harnessed by evaluating thicker sample volumes, overlaying images acquired from multiple areas to evaluate larger regions, including more time points, and evaluating more targets of interest. Additional markers, such as smooth muscle myosin heavy chain, vimentin, and smoothelin, can be explored to provide more definitive markers of SMC lineage as well as to rigorously describe the SMC phenotype changes occurring throughout aneurysm development (Chen et al. 2006; Rensen et al. 2007; Ailawadi et al. 2009). More cell types, such as macrophages, can be evaluated to explore the role of inflammation in aneurysm progression. Finally, additional types of collagen, such as collagen type III, can be characterized to understand the role of unique collagen types in the remodeling and repair of the vessel wall.

In summary, we have applied a novel microscopy technology, IAT, to the elastase-perfusion murine AAA model. In comparison to traditional microscopy technology, IAT, coupled with custom quantification algorithms, has enabled precise and detailed quantification of the content, microstructure, and organization of the complex 3D vessel wall environment with minimal subjectivity (Yamaguchi et al. 2000; Dai et al. 2006). The spatial and temporal investigation helped elucidate the unique dynamics of remodeling during aneurysm development and progression. High-resolution 3D volumetric information may provide a new perspective into AAA pathology, whereas quantitative depictions may prove useful for the development of models describing elastin degradation and fragmentation, the interaction of multiple tissue constituents, and the kinetics of ECM growth and remodeling. Future work may probe deeper into exploring the mechanisms of and key biological processes involved in both AAA development and other forms of cardiovascular disease.

Acknowledgments

The authors gratefully acknowledge all members of Professor Stephen J Smith's laboratory at Stanford University, especially Brad L. Busse, Dr. Kristina D. Micheva, Dr. Nancy A. O'Rourke, and Dr. Gordon X. Wang, for their technical expertise in IAT. The authors also gratefully acknowledge all staff members of the Cell Sciences Imaging Facility at Stanford University, especially Jon W. Mulholland and Ibanri Phanwar, for technical guidance and all array generation. We would also like to acknowledge Dr. Andrew

J. Connolly and Amarjeet Grewall in the Pathology Department and Pauline Chu in the Comparative Medicine Department at Stanford University for their expertise in vascular histology and immunohistochemistry. We also acknowledge Dr. Joan M. Greve for her encouragement, support, and critical review of the manuscript.

Declaration of Conflicting Interests

The authors declared no potential conflicts of interest with respect to the authorship and/or publication of this article.

Funding

The authors disclosed receipt of the following financial support for the research and/or authorship of this article: S. Saatchi was supported by a Stanford University Bio-X Graduate Student Fellowship sponsored by Amgen, Inc. This research was funded in part by the National Institutes of Health to CAT and PST (1P50HL083800) and the California Tobacco Related Disease Research Program to PST (18XT-0174). The authors do not have any conflicts of interest.

References

Acampora KB, Nagatomi J, Langan EM III, LaBerge M. 2010. Increased synthetic phenotype behavior of smooth muscle cells in response to in vitro balloon angioplasty injury model. Ann Vasc Surg. 24(1):116–126.

Ailawadi G, Moehle CW, Pei H, Walton SP, Yang Z, Kron IL, Lau CL, Owens GK. 2009. Smooth muscle phenotypic modulation is an early event in aortic aneurysms. J Thorac Cardiovasc Surg. 138(6):1392–1399.

Anidjar S, Salzmann JL, Gentric D, Lagneau P, Camilleri JP, Michel JB. 1990. Elastase-induced experimental aneurysms in rats. Circulation. 82(3):973–981.

Azuma J, Asagami T, Dalman R, Tsao PS. 2009. Creation of murine experimental abdominal aortic aneurysms with elastase. J Vis Exp. 29:1280.

Bunton TE, Biery NJ, Myers L, Gayraud B, Ramirez F, Dietz HC. 2001. Phenotypic alteration of vascular smooth muscle cells precedes elastolysis in a mouse model of Marfan syndrome. Circ Res. 88(1):37–43.

Chen CN, Li YS, Yeh YT, Lee PL, Usami S, Chien S, Chiu JJ. 2006. Synergistic roles of platelet-derived growth factor-BB and interleukin-1beta in phenotypic modulation of human aortic smooth muscle cells. Proc Natl Acad Sci U S A. 103(8):2665–2670.

Cho BS, Roelofs KJ, Ford JW, Henke PK, Upchurch GR Jr. 2010. Decreased collagen and increased matrix metalloproteinase-13 in experimental abdominal aortic aneurysms in males compared with females. Surgery. 147(2):258–267.

Clark JM, Glagov S. 1985. Transmural organization of the arterial media: the lamellar unit revisited. Arteriosclerosis. 5(1): 19–34.

Dai D, Ding YH, Lewis DA, Kallmes DF. 2006. A proposed ordinal scale for grading histology in elastase-induced, saccular aneurysms. AJNR Am J Neuroradiol. 27(1):132–138.

Davies JQ, Gordon S. 2005. Isolation and culture of murine macrophages. Methods Mol Biol. 290:91–103.

Dingemans KP, Teeling P, Lagendijk JH, Becker AE. 2000. Extracellular matrix of the human aortic media: an ultrastructural histochemical and immunohistochemical study of the adult aortic media. Anat Rec. 258(1):1–14.

Fleming C, Whitlock EP, Beil TL, Lederle FA. 2005. Screening for abdominal aortic aneurysm: a best-evidence systematic review for the U.S. preventive services task force. Ann Intern Med. 142:203–211.

Humphrey JD, Taylor CA. 2008. Intracranial and abdominal aortic aneurysms: similarities, differences, and need for a new class of computational models. Annu Rev Biomed Eng. 10:221–246.

Iwata H, Sata M. 2008. Origin of cells that contribute to neointima growth. Circulation. 117(24):3060–3061.

Jacob MP, Badier-Commander C, Fontaine V, Benazzoug Y, Feldman L, Michel JB. 2001. Extracellular matrix remodeling in the vascular wall. Pathol Biol (Paris). 49(4):326–332.

Lopez-Candales A, Holmes DR, Liao S, Scott MJ, Wickline SA, Thompson RW. 1997. Decreased vascular smooth muscle cell density in medial degeneration of human abdominal aortic aneurysms. Am J Pathol. 150(3):993–1007.

Menashi S, Campa JS, Greenhalgh RM, Powell JT. 1987. Collagen in abdominal aortic aneurysm: typing, content, and degradation. J Vasc Surg. 6(6):578–582.

Micheva KD, Smith SJ. 2007. Array tomography: a new tool for imaging the molecular architecture and ultrastructure of neural circuits. Neuron. 55(1):25–36.

O'Connell MK, Murthy S, Phan S, Xu C, Buchanan J, Spilker R, Dalman RL, Zarins CK, Denk W, Taylor CA. 2008. The three-dimensional micro- and nanostructure of the aortic medial lamellar unit measured using 3D confocal and electron microscopy imaging. Matrix Biol. 27(3):171–181.

Owens GK, Kumar MS, Wamhoff BR. 2004. Molecular regulation of vascular smooth muscle cell differentiation in development and disease. Physiol Rev. 84(3):767–801.

Pyo R, Lee JK, Shipley JM, Curci JA, Mao D, Ziporin SJ, Ennis TL, Shapiro SD, Senior RM, Thompson RW. 2000. Targeted gene disruption of matrix metalloproteinase-9 (gelatinase B) suppresses development of experimental abdominal aortic aneurysms. J Clin Invest. 105(11):1641–1649.

Rensen SS, Doevendans PA, van Eys GJ. 2007. Regulation and characteristics of vascular smooth muscle cell phenotypic diversity. Neth Heart J. 15(3):100–108.

Rizzo RJ, McCarthy WJ, Dixit SN, Lilly MP, Shively VP, Flinn WR, Yao JS. 1989. Collagen types and matrix protein content in human abdominal aortic aneurysms. J Vasc Surg. 10(4):365–373.

Saatchi S, Wanchoo N, Azuma J, Smith SJ, Tsao PS, Yock PG, Taylor CA. 2011. The use of immunofluorescent array tomography to study the three-dimensional microstructure of murine blood vessels. Cell Mol Bioeng. 4(2):311–323.

Sinha I, Cho BS, Roelofs KJ, Stanley JC, Henke PK, Upchurch GR Jr. 2006. Female gender attenuates cytokine and chemokine expression and leukocyte recruitment in experimental rodent abdominal aortic aneurysms. Ann N Y Acad Sci. 1085:367–379.

Thompson RW, Curci JA, Ennis TL, Mao D, Pagano MB, Pham CT. 2006. Pathophysiology of abdominal aortic aneurysms: insights from the elastase-induced model in mice with different genetic backgrounds. Ann N Y Acad Sci. 1085:59–73.

Thompson RW, Liao S, Curci JA. 1997. Vascular smooth muscle cell apoptosis in abdominal aortic aneurysms. Coron Artery Dis. 8(10):623–631.

Yamaguchi T, Yokokawa M, Suzuki M, Higashide S, Katoh Y, Sugiyama S, Misaki T. 2000. The time course of elastin fiber degeneration in a rat aneurysm model. Surg Today. 30(8):727–731.